The Astrophysical Journal, 629:L133–L136, 2005 August 20

LARGE-AMPLITUDE VELOCITY FLUCTUATIONS IN CORONAL LOOPS: FLARE DRIVERS?

G. Nigro, F. Malara, and P. Veltri
Università della Calabria, Dipartimento di Fisica, I-87036 Arcavacata di Rende, Italy; nigro@fis.unical.it, malara@fis.unical.it, veltri@fis.unical.it
Received 2005 March 21; accepted 2005 July 13; published 2005 August 5

ABSTRACT

Recent space observations of coronal lines broadening during a flare occurrence suggest that unresolved nonthermal velocity rises well above the background level before the start of the flare, defined as the start of hard X-ray emission. Using a new shell model to describe the Alfvénic turbulence inside a coronal loop, it is shown that the occurrence of high values (of the order of 100 km s^{-1}) of the large-scale fluctuating velocity can represent an efficient trigger to a nonlinear intermittent turbulent cascade and then to the generation of a burst of dissipated energy. The numerical results of the model furnish a well-supported physical explanation for the reason why large velocity fluctuations represent the flare trigger rather than the result of the later energy deposition.

Subject headings: plasmas — Sun: activity — Sun: corona

1. INTRODUCTION

Some years ago Parker (1988) put forward the concept of "nanoflares" (i.e., flares characterized by an energy $\sim 10^{24}$ ergs), in order to furnish a unified view of the flare and coronal heating problems. He postulated that the interaction between the forcing motions of the photosphere and the dynamics created by the coronal magnetic field and plasma could give rise to energy releases resulting from the cumulative effect of reconnection inside many small-scale discrete current sheets; these events should make up the majority of the heat that is deposited in the solar atmosphere. Notwithstanding the large popularity of Parker's idea, models describing flares have rarely studied the problem of the physical mechanism that triggers the reconnection process, and almost no observational prediction about this mechanism has been derived (Feldman et al. 2003).

Recently, Nigro et al. (2004) have built up a new *hybrid shell* model to describe the resonant storage of fluctuating magnetic and kinetic energy in a coronal loop and their subsequent dissipation due to small-scale formation through a nonlinear cascade. The intermittent behavior of turbulence described by the model gives rise to bursts of dissipation whose statistics compare rather well with that of the hard X-ray (HXR) emission associated with solar flares. Moreover, since energy stored in the form of magnetic field fluctuations can represent a significant fraction (5%) of the background magnetic field energy, the model can also reproduce relatively energetic flares, provided they do not destroy the loop structure. It is then worth analyzing the recent investigation of nonthermal mass motions in the solar corona in coincidence with flares and comparing them to the model predictions by Nigro et al. (2004) in order to see if they could provide a key to understanding flare and coronal heating mechanisms.

It has been found that during flares, the emission lines are broader than the thermal width; this broadening corresponds to a nonthermal velocity of the order of 100 km s^{-1} (Doschek 1983; Antonucci et al. 1984). Alexander et al. (1998) have tried to determine when the nonthermal velocity peaks occur relative to HXR bursts. They have analyzed 10 flares and found that the nonthermal velocity measured from S XV spectra exhibits a peak prior to the first significant HXR peak or is already decaying from an earlier unobserved peak. These results suggest that the large values of nonthermal velocity are related to the actual flare trigger rather than to the later energy deposition. Mariska & McTiernan (1999) have also found that early in the flare, the nonthermal velocity is at or near its peak value for the event, and it then generally declines throughout the flare; however, when it is possible to measure the peak of nonthermal velocity derived from Ca XIX spectra, it occurs after the first significant peak in HXRs. Harra et al. (2001) discuss the observations of two flares; they find an increase in values of nonthermal velocity before the start of the flare. Although there is no significant preflare change in the Bragg Crystal Spectrometer light-curve or temperature change, there is a strong preflare signature in the line broadening. They suggest therefore that there is preflare turbulence associated with the process that eventually triggers the flare. A large statistical study has been carried out by Ranns et al. (2001) analyzing 59 limb flares. They found that the time delay between the peaks of the HXR and nonthermal velocity is related to the number of subsidiary HXR peaks before the main peak. In the gradual-rise flares, nonthermal velocities tend to peak before HXRs do, whereas the opposite behavior is observed in impulsive flares.

In any case, several observations support the view that the rise in the nonthermal velocity above the background level occurs before the start of the flare, defined as the start of the HXR emission, suggesting that this increase is an indicator of turbulent changes in the plasma of the region prior to the flare and that it is related to the flare trigger mechanism. In this Letter we analyze the behavior of the velocity fluctuations predicted by the Nigro et al. (2004) model in order to perform an effective comparison with the above reported observations.

2. THE REDUCED MHD SHELL MODEL FOR TURBULENCE IN CORONAL LOOP

In a highly simplified form, a loop can be represented as a box, with a large aspect ratio $R = L/L_\perp \gg 1$ (L being the height and $L_\perp$ the side of its square basis), inside which there is a region of uniform density ρ and uniform magnetic field $\boldsymbol{B}_0$. Nigro et al. (2004) have studied the energy input in the form of Alfvén waves in the above-described loop model and the subsequent evolution of the MHD turbulence inside, using a set of equations, which they refer to as the *hybrid shell model*. The small coronal value of kinetic-to-magnetic pressure ratio ($\beta \sim 10^{-2}$) and the large aspect ratio of coronal loops allow one to retain only the noncompressive components of velocity and magnetic field fluctuations perpendicular to $\boldsymbol{B}_0$; only propagation at the Alfvén speed takes place in the direction parallel to $\boldsymbol{B}_0$ (the reduced MHD approximation; Strauss 1976; Zank

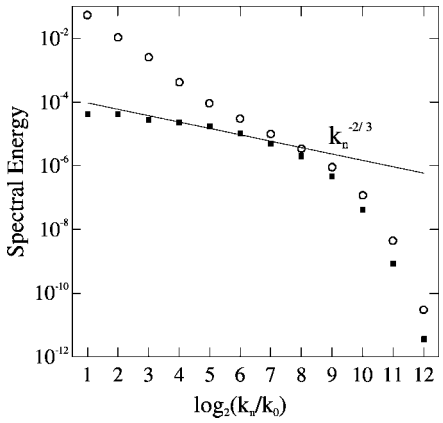

FIG. 1.—Normalized kinetic (*filled squares*) and magnetic (*open circles*) spectral energy as a function of the shell order. The spectra are averaged both in direction along the loop and in time.

& Matthaeus 1992). A Fourier transform in the two coordinates perpendicular to $\boldsymbol{B}_0$ is performed, but the dependence on the space variable x along $\boldsymbol{B}_0$ is kept. The model is then built up by following a standard procedure (Giuliani & Carbone 1998): the $\boldsymbol{k}$-space perpendicular to $\boldsymbol{B}_0$ is divided into concentric shells of exponentially growing radius; for each shell, a scalar value $k_n = k_0 2^n$ ($k_0 = 2\pi/L_\perp$) of the wavevector and scalar values $v_{\perp n}(x, t)$ and $b_{\perp n}(x, t)$ of the perpendicular velocity and magnetic field variables are defined. The evolution equations for these dynamical variables are derived and presented elsewhere (Nigro et al. 2004). Most of the energy in photospheric motions is concentrated at larger spatial scales $\sim L_\perp$, and at the lower boundary only the first three shells are excited with random signals that are Gaussian-distributed, with an amplitude of $\sim$1 km s^{-1} and a correlation time of $\sim$5 minutes, reproducing photospheric motions. Total reflection is imposed at both boundaries.

The model equations have been numerically solved, in a typical case characterized by a parallel length $L = 3 \times 10^4$ km, an aspect ratio $R = 30/2\pi$, an Alfvén velocity $c_A = 2 \times 10^3$ km s^{-1}, and a mass density $\rho = 1.67 \times 10^{-16}$ g cm^{-3}. A very small dimensionless dissipation coefficient $\chi = \mu/(c_A L) = 10^{-7}$ has been used (the magnetic diffusivity μ being assumed equal to the kinematic viscosity ν).

The fluid motions at the base of the loop inject Alfvénic fluctuations, which gradually fill the whole structure, storing magnetic and kinetic energy inside it. The presence of these fluctuations is consistent with SUMER/*SOHO* observations of the behavior of center-to-limb nonthermal line broadening (Erdelyi et al. 1998; Doyle et al. 2000). This broadening, in fact, suggests that the nonthermal motions are nonisotropic in the transition region and in the upper chromosphere, with the horizontal (tangential to the solar surface) unresolved motions exceeding those in the vertical plane. The presence of transverse polarized fluctuations could then explain the different behavior.

When the energy level has become sufficiently high, nonlinear couplings transfer this energy to smaller scales in the transverse direction. In this way a spectrum is formed (Fig. 1), ranging from the large injection scales ($n \leq 2$) down to the small dissipative scales ($n \geq 9$). In the inertial domain ($3 \leq n \leq 8$) the characteristic Kolmogorov power-law spectrum is displayed by kinetic energy. Magnetic field fluctuations dominate over velocity fluctuations (Einaudi & Velli 1999) at least at large scales ($\delta B_\perp/B_0 \simeq 0.2$ and $\delta v_\perp/c_A \simeq 10^{-2}$). Nevertheless, the velocity fluctuations inside the loop are considerably larger

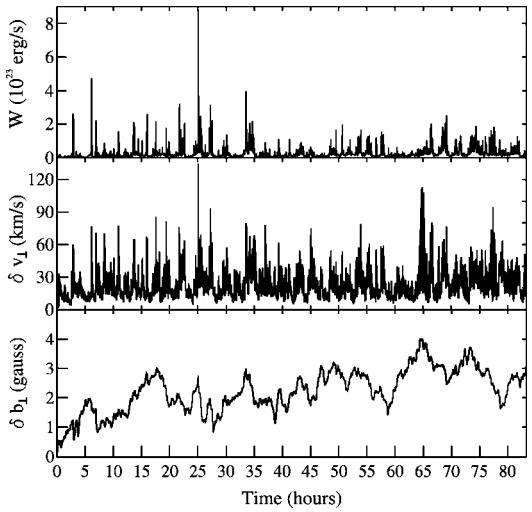

FIG. 2.—The rms value of the velocity (*middle panel*) and magnetic field (*lower panel*) fluctuations as a function of time. The dissipated power is represented in upper panel for comparison.

than the photospheric motions, which shows that the loop works as an efficient energy storage device.

The time dependence of dissipated power shown in Figure 2 displays a sequence of spikes, which are supposed to represent the energy release events observed in the solar corona. The statistical properties of such events (probability distributions for peak maximum power, burst duration time, energy dissipated in a burst, and waiting time between bursts) compare satisfactory with the observed properties of coronal flares (Nigro et al. 2004).

3. VELOCITY FLUCTUATIONS

An important test for the model is represented by the comparison of velocity fluctuations obtained in the numerical model with observations of unresolved nonthermal velocity, which represents the excess amount of an observed line width over the thermal contribution. In the framework of our model we can interpret the observed nonthermal velocity as turbulent velocity since nonthermal motion is characterized by disordered variations occurring on very small scales.

The time-averaged velocity distribution along the loop is represented in Figure 3: starting from about 1 km s^{-1} at the boundary, values of the order of 30 km s^{-1} are obtained 3000 km higher. These numerical values are in agreement with the observed coronal nonthermal velocity obtained by Brosius et al.

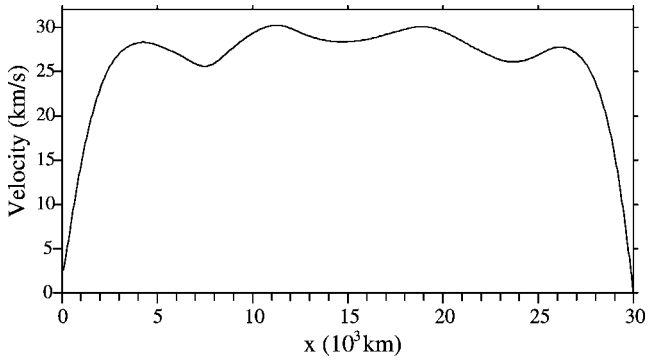

FIG. 3.—The rms value of the velocity fluctuations as a function of the coordinate along the loop.

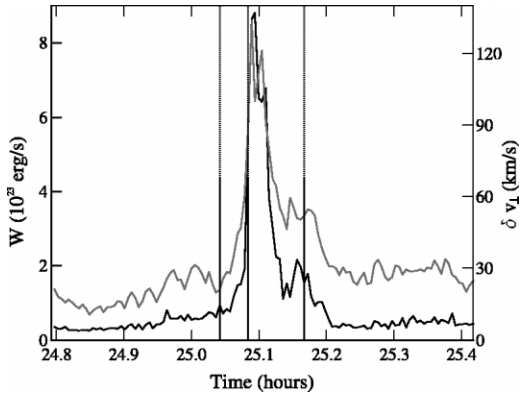

FIG. 4.—Velocity fluctuations (*dotted gray line*) and dissipated power (*solid black line*) time evolution in correspondence with a burst of dissipation. The spectra presented in Fig. 5 are calculated at the times corresponding to the vertical lines.

(2000), who, using the strong emission line observed for each ionization stage of Fe X–XVI and Ni XVIII, find that all nonthermal line widths yield velocities consistent with 35 km s^{-1}.

The distribution of velocity fluctuations as a function of the altitude can be compared with the distribution of unresolved velocity, observed by the SUMER experiment (Chae et al. 1998). Assuming that temperature is directly related to height above the photosphere, it is seen that unresolved nonthermal velocities grow from about 1 km s^{-1} at $T \sim 10^4$ K up to 30 km s^{-1} at $T \sim 3 \times 10^5$. For higher temperatures, velocities decrease. The increase of unresolved nonthermal velocity with height above the photosphere has also been observed by Doyle et al. (1998) up to an altitude of about 25,000 km above the equatorial limb. Harrison et al. (2002) have made a study that is complementary to the Doyle et al. (1998) study, looking at an altitude 6 times greater. By analyzing EUV line widths in the equatorial quiet corona up to an altitude of 150,000 km off-limb, they show that an emission line narrows as a function of altitude above 50,000 km. On the whole, these observations are consistent with the idea that the amplitude of velocity fluctuations increases with altitude inside the coronal loops and remains relatively low outside the coronal loops, thus showing that coronal loops are able to store energy in the form of velocity and magnetic fluctuations transverse to the background magnetic field.

Even more interesting comparisons may be derived from the analysis of nonthermal velocity measured in correspondence with flares. Considering the time behavior of velocity fluctuations in our numerical simulations (Fig. 2), it is seen that while magnetic field fluctuations display variations on timescales of the order of several hours, much the same as stored fluctuating energy, velocity fluctuations are characterized by spikes that can be as high as 80–140 km s^{-1}, much larger then their average value ($\simeq$30 km s^{-1}). Even if these spikes are not always correlated with a burst of dissipation, the contrary is always true: every dissipation burst correlates with a spike in the velocity fluctuation. The strong increase of velocity fluctuations in correspondence with a dissipation burst (Fig. 4) compares extremely well with the increase of nonthermal velocity observed during flares. In fact, Landi et al. (2003) have observed a maximum value of ~100 km s^{-1} at flare onset and then a decay to the value of ~30 km s^{-1}, typical of nonthermal mass motion for nonflaring plasma.

It is worth trying to understand why large values of velocity fluctuations seem to be necessary for driving the dissipation

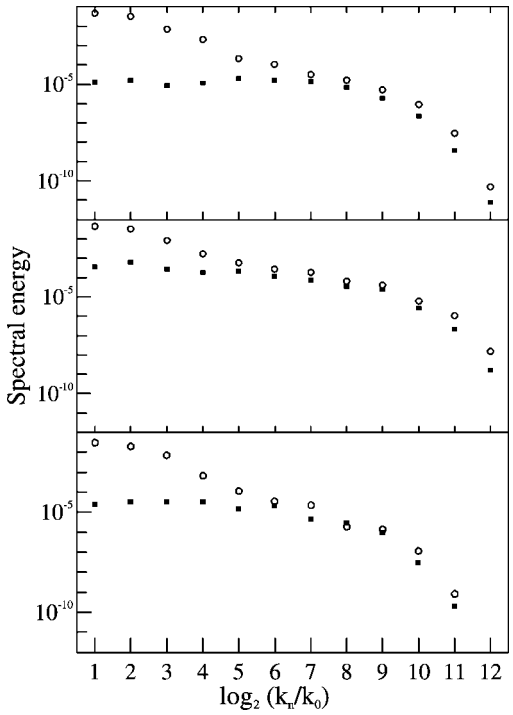

FIG. 5.—Normalized kinetic (*filled squares*) and magnetic (*open circles*) spectral energy as a function of the shell order. Spectra are averaged in the loop direction and calculated at three different times indicated by the vertical lines in Fig. 4.

bursts. Since fluctuating magnetic energy is always much larger than fluctuating kinetic energy, the energy flow per mass unit Π_ℓ at a given length scale ℓ, which represents a third-order moment of fluctuations, can be estimated, by retaining only the leading term, as

$$\Pi_\ell \simeq \frac{\delta b_\ell^2 \delta v_\ell}{\ell} \tag{1}$$

(no term proportional to δb_ℓ^3 is obviously present in the energy flow). A physical interpretation of equation (1) can be given by noting that the energy density δb_ℓ^2 is transferred along the spectrum with the typical turnover time of velocity fluctuations $\tau_\ell \simeq \ell/\delta v_\ell$. Π_ℓ is constant along the spectrum, as a function of ℓ, so that its value is determined by the energy injection rate, i.e., the value it assumes at the injection scale $L_\perp$. Since the energy of magnetic fluctuations at large scales, after the initial transient, remains more or less constant, an increase of the velocity fluctuation amplitude at large scales could result in a strong reduction in the turnover time and thus in a sudden increase of the spectral energy flow toward small scales, which in turn could give rise to a spike in the dissipated energy. For this reason, the increase in the values of the velocity fluctuations at large scales can represent a trigger of flares.

This phenomenology is clearly observed in Figure 4, where it is seen that the burst of dissipation starts just after the growth of the velocity fluctuation. In Figure 5, it is also seen that the large-scale kinetic energy, which is much lower than the magnetic energy before the dissipation burst (*top panel*), approaches the level of magnetic energy just before the start of the dissipation burst (*middle panel*). At the same time, both the kinetic energy level and the magnetic energy level on dissipative scales increase by more than 2 orders of magnitude. After the dissipation burst, the kinetic energy at large scales once again

becomes much lower than the magnetic energy (*bottom panel*), while energy level on dissipative scales decreases to values smaller than those in the preflare phase. High values of the third-order correlation in the spectral flow expression (eq. [1]) require a peculiar phase relation between magnetic and kinetic fluctuations. This could explain why it is that not every velocity spike gives rise to a dissipation burst.

4. OBSERVING RECONNECTION

Since the most popular reconnection models (Sweet 1958; Parker 1957; Petschek 1964) predict bidirectional outflow jets, great efforts have been made to observe them. Cargill (1996) synthesized coronal spectral line profiles associated with the nanoflare model. His computations of spectral line profiles produced by reconnection outflows, which could arise in nanoflares, predict Doppler shifts or line broadening in excess of those observed. Possible bidirectional outflow jets have been indeed observed in SUMER data (Innes et al. 1997; Wilhelm et al. 1998), but the measured temperatures are more consistent with chromospheric reconnection than with coronal reconnection; moreover, the velocities are much slower than what was expected (Curdt et al. 1998). Klimchuk (1998), on the other hand, raises the question as to whether or not the reconnection outflow in the corona is bright enough to be observed by present-day instrumentation and concludes that it is much too faint.

The *hybrid shell model* that we have used does not allow for a description of the spatial characteristics of turbulence. Nevertheless, some information about the nature of the intermittent dissipative structures of MHD turbulence can be derived from solar wind data analysis (Veltri & Mangeney 1999), where these structures have been identified as current sheets. The shell model furnishes the typical scale of these sheets, which is of the order of the dissipative scale, i.e., many orders of magnitude smaller than $L_\perp$. This means that the regions where dissipated energy is deposited are very thin perpendicular to $\boldsymbol{B}_0$. This result could explain why the efforts to observe outflow jets, generated in coronal reconnection events, have not been successful: the current sheets produced by nonlinear cascade occur at a scale that is far beyond the possibility of instrumental resolution. Due to wave propagation, the region where dissipation occurs can be very long in the direction parallel to $\boldsymbol{B}_0$. This heating model then gives rise to an energy deposition that concerns only a narrow bundle of field lines and therefore is consistent with the abundance of very fine scale structures in the *TRACE* images (Aschwanden et al. 2000).

REFERENCES

Alexander, D., Harra-Murnion, L. K., Khan, J. I., & Matthews, S. A. 1998, ApJ, 494, L235
Antonucci, E., Gabriel, A. H., & Dennis, B. R. 1984, ApJ, 287, 917
Aschwanden, M. J., Nightingale, R. W., & Alexander, D. 2000, ApJ, 541, 1059
Brosius, J. W., Thomas, R. J., Davila, J. M., & Landi, E. 2000, ApJ, 543, 1016
Cargill, P. J. 1996, Sol. Phys., 167, 267
Chae, J., Schhle, U., & Lemaire, P. 1998, ApJ, 505, 957
Curdt, W., Innes, D. E., & Wilhelm, K. 1998, in Solar Jets and Coronal Plumes, ed. T.-D. Guyenne (ESA SP-421; Noordwijk: ESA), 123
Doschek, G. A. 1983, Sol. Phys., 86, 9
Doyle, J. G., Banerjee, D., & Perez, M. E. 1998, Sol. Phys., 181, 91
Doyle, J. G., Teriaca, L., & Banerjee, D. 2000, A&A, 356, 335
Einaudi, G., & Velli, M. 1999, Phys. Plasmas, 6, 4146
Erdelyi, R., Doyle, J. G., Perez, M. E., & Wilhelm, K. 1998, A&A, 337, 287
Feldman, U., Landi, E., & Curdt, W. 2003, ApJ, 585, 1087
Giuliani, P., & Carbone, V. 1998, Europhys. Lett., 43, 527
Harra, L. K., Matthews, S. A., & Culhane, J. L. 2001, ApJ, 549, L245
Harrison, R. A., Hood, A. W., & Pike, C. D. 2002, A&A, 392, 319
Innes, D. E., Inhester, B., Axford, W. I., & Willhelm, K. 1997, Nature, 386, 811
Klimchuk, J. A. 1998, in Solar Jets and Coronal Plumes, ed. T.-D. Guyenne (ESA SP-421; Noordwijk: ESA), 233
Landi, E., Feldman, U., Innes, D. E., & Curdt, W. 2003, ApJ, 582, 506
Mariska, J. T., & McTiernan, J. M. 1999, ApJ, 514, 484
Nigro, G., Malara, F., Carbone, V., & Veltri, P. 2004, Phys. Rev. Lett., 92, 194501
Parker, E. N. 1957, J. Geophys. Res., 62, 509
———. 1988, ApJ, 330, 474
Petschek, H. E. 1964, in The Physics of Solar Flares, ed. W. N. Hess (NASA SP-50; Washington, DC: NASA), 425
Ranns, N. D. R., Harra, L. K., Matthews, S. A., & Culhane, J. L. 2001, A&A, 379, 616
Strauss, H. 1976, Phys. Fluids, 19, 134
Sweet, P. A. 1958, in IAU Symp. 6, Electromagnetic Phenomena in Cosmical Physics, ed. B. Lehnert (New York: Cambridge Univ. Press), 123
Veltri, P., & Mangeney, A. 1999, in AIP Conf. Proc. 471, Solar Wind Nine, ed. S. R. Habbal et al. (Woodbury: AIP), 543
Wilhelm, K., Innes, E. E., Curdt, W., Kliem, B., & Brekke, P. 1998, in Solar Jets and Coronal Plumes, ed. T.-D. Guyenne (ESA SP-421; Noordwijk: ESA), 103
Zank, G. P., & Matthaeus, W. H. 1992, J. Plasma Phys., 48, 85